Mixing Thermodynamics of the Calcite-Structured (Mn,Ca)CO3 Solid Solution: A Computer Simulation Study

ARTICLE *in* THE JOURNAL OF PHYSICAL CHEMISTRY B · DECEMBER 2011

Impact Factor: 3.3 · DOI: 10.1021/jp200378q · Source: PubMed

3 AUTHORS, INCLUDING:

Ricardo Grau-Crespo
University of Reading
72 PUBLICATIONS **772** CITATIONS
SEE PROFILE

Nora H. de Leeuw
Cardiff University
240 PUBLICATIONS **4,428** CITATIONS
SEE PROFILE

THE JOURNAL OF PHYSICAL CHEMISTRY B

ARTICLE

pubs.acs.org/JPCB

Mixing Thermodynamics of the Calcite-Structured $(Mn,Ca)CO_3$ Solid Solution: A Computer Simulation Study

Qi Wang, Ricardo Grau-Crespo, and Nora H. de Leeuw*

Department of Chemistry, University College London, 20 Gordon Street, London WC1H 0AJ, United Kingdom

ABSTRACT: We have employed atomistic simulation techniques to investigate the thermodynamics of mixing in the solid solutions of calcite ($CaCO_3$) and rhodochrosite ($MnCO_3$). Our calculations show that the fully disordered solid solution has positive enthalpies of mixing for the entire range of compositions, which confirm recent experiments. The consideration of a small degree of ordering in the simulations leads to mixing enthalpies in quantitative agreement with experimental measurements. We argue that earlier measurements of negative mixing enthalpies for the Mn-rich solid solution were probably due to relatively high degrees of ordering in the samples. Our calculations show that the lowest energy configuration for each composition is always the one that maximizes the homogeneity of the cations within (0001) layers but maximizes the heterogeneity across layers. In particular, for Mn/Ca = 1, the most stable configuration corresponds to the ordered structure of kutnahorite, where layers of Ca and Mn ions alternate along the *c* axis, similar to the Ca/Mg ordering in dolomite. Our simulations predict that kutnahorite becomes less stable than the fully disordered 50:50 solid solution at ~850 K, and this disordering temperature decreases to a value in better agreement with experiment (695 K), if a transition to a partially ordered structure is considered. Our results thus suggest that the "disordered" $(Mn,Ca)CO_3$ solid solutions, which are known to be favored by kinetic factors, are actually not fully disordered, but contain a higher abundance of lower-energy cation arrangements than that expected from a completely random distribution.

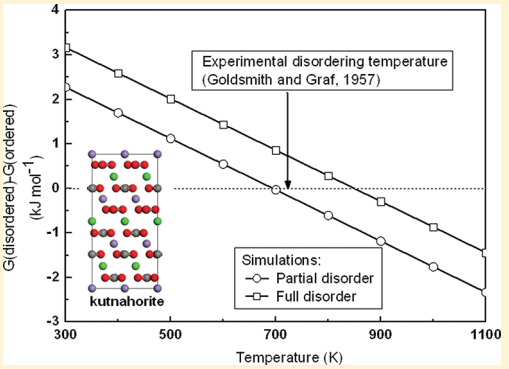

INTRODUCTION

Manganese is one of the most toxic metals found in soils and rocks. Dissolved manganese from natural sources or carcinogenic industrial waste may contaminate groundwater.[1−3] The geochemical cycle of manganese involves rock weathering, microbial activity, dissolution into natural water and formation of manganese-containing minerals, where the mobility of manganese in the cycle can be controlled by its incorporation into minerals such as calcite.[4,5] During this process, calcite takes up the dissolved manganese via dissolution-recrystallization processes which frequently involve the formation of solid solutions, where the maximum solubility of Mn^{2+} is controlled by its reaction with calcite and the mixing thermodynamics of the $(Mn,Ca)CO_3$ solid solutions.[6,7] The investigation of the properties of this solid solution is thus useful to gain insight into the flux of manganese in the environment.

Although the mixed carbonates $Mn_xCa_{1-x}CO_3$ have been widely studied using experimental techniques, such as solution calorimetry, seemingly contradictory results are still reported in the literature, particularly with respect to the range of the miscibility gap at different temperatures and the sign of the mixing thermodynamic potentials. For example, Goldsmith and Graf reported the existence of a miscibility gap for $0.6 < x < 0.75$ at ambient temperatures and suggested that complete miscibility only occurs above 823 K,[8,9] whereas De Capitani and Peters studied the solvus in the $Mn_xCa_{1-x}CO_3$ system and found that the critical point lies at 813 K with a miscibility gap of $0.5 < x < 0.9$ at 623 K.[10] In contrast, other studies that have analyzed samples of natural and synthetic origin have found that the miscibility gap covers most of the Mn compositional range at room temperature.[11−13] The mixing enthalpies in the Mn-rich region have been reported to be negative by Capobianco and Navrotsky,[14] but positive values have been found for the same compositions in a recent study by Katsikopoulos et al.[15]

The intermediate composition $Ca_{0.5}Mn_{0.5}CO_3$ and the stability of the ordered phase with this composition (kutnahorite) at different temperatures also leaves a number of unanswered questions. For example, Capobianco and Navrotsky reported a positive free energy of mixing for the $Ca_{0.5}Mn_{0.5}CO_3$ system at high temperature,[14] while McBeath and co-workers measured a negative value at 298 K.[13] Furthermore, whereas the ordered kutnahorite structure has been found in previous work,[9,10,13] Katsikopoulos et al. have indicated that this structure is not likely to precipitate at ambient temperatures, and their X-ray diffraction experiments did not show the clear superstructure reflections typical of kutnahorite ordering.[15] These authors argue that these incompatible results are probably due to kinetic factors, such as precipitation rate and phase equilibrium at high supersaturation, which are difficult to control in experiments.

Received: January 13, 2011
Revised: October 17, 2011
Published: October 19, 2011

As an effective complementary technique to experiment, computer modeling can be used to study complex mineral structures and processes at the atomic level, including the formation of solid solutions, where it is possible to access the thermodynamic properties without the effect of unknown kinetic factors. Interatomic potential models, in particular, have been used extensively to simulate the structure and properties of rhombohedral carbonates.[16−23] These studies have demonstrated the suitability of molecular simulation in providing a theoretical description of complex bulk and surface processes in carbonates and how the theoretical models assist experiment in the evaluation and interpretation of observations. The thermodynamics of the $(Ca,Mn)CO_3$ system (and also of the tertiary system including Mg besides Ca and Mn) have been discussed in a recent paper by Vinograd et al.,[24] where a pairwise interaction model is employed to perform Monte Carlo simulations in a very large supercell of the structure, allowing full convergence of the calculations with respect to cell size. In the present paper we have focused on the $(Ca,Mn)CO_3$ binary system, following a different approach, which is based on the calculation of all inequivalent site occupancy configurations in a smaller supercell. This allows us to keep an accurate description of the interatomic interactions and include relaxation effects explicitly in our simulations. It also enables the calculation of effective properties beyond the energy, based on configurational averages (for example, effective cell parameters as a function of composition), and to evaluate easily the contribution of vibrational effects. Due to the restrictions in supercell size inherent in our method, we focus here on the behavior of the mixing enthalpy of the solid solution, which exhibits a rapid convergence with cell size. Our results are then compared with experimental measurements using calorimetric methods.

METHODS

We have employed atomistic simulation methods based on the Born model of solids,[25] which assumes that the ions in the solid interact via long-range electrostatic forces and short-range forces. The short-range interactions, such as electron cloud repulsions and van der Waals interactions are described by a Buckingham potential. Covalent interactions within the carbonate group are modeled by a Morse potential, a three-body angular potential and a four-body dihedral potential. The electronic polarizability of the ions is included via the shell model of Dick and Overhauser,[26] in which each polarizable ion (i.e., the oxygen in CO_3^{2-}) is presented by a core and a massless shell, connected by a spring. The polarizability of the ion is then determined by the spring constant and the charges of the core and shell.

The $CaCO_3$ potential parameters employed in this study (Table 1) were originally derived by Pavese et al.[27] and were slightly modified later for a better description of the covalent bonding in the carbonate ion.[28] It has been found that they correctly describe the structural, vibrational, and thermal properties of both calcite and aragonite.[27−29] The interatomic potential parameters for the Mn^{2+} were derived using the computer code GULP,[30−32] where the parameters are fitted to the crystal structure and the bulk modulus by a penalty minimization scheme. The experimental hexagonal unit cell volumes of $CaCO_3$ and $MnCO_3$ are 367.8 and 307.8 Å^3, and following the approach used by de Leeuw and co-workers in their derivation of MCO_3 potentials (where M = Mg, Cd, Sr, Fe),[33,34] when fitting the interatomic potentials we required the relative unit cell volumes to retain the experimental ratio of Ca:M_n = 1:0.84. Furthermore, in order to obtain reliable relative lattice structure and energies for the solid solutions, we required the relative energies of formation of the end-members $CaCO_3$ and $MnCO_3$ to be comparable to experiment, where we have considered the enthalpy of the following reaction:

$$Ca^{2+}(g) + MnCO_3(s) \rightarrow Mn^{2+}(g) + CaCO_3(s) \quad (1)$$

The derived potential parameters reproduce the enthalpy of the above reaction to within 2% of the experimental enthalpy (Table 2). In this calculation we included vibrational (both zero-point and heat capacity) contributions to the enthalpies, although we found that they represent only 1.3 kJ/mol (0.5%) of the reaction enthalpy. The calculated structural parameters of the Ca and Mn end-members are compared with experiment in Table 2, and these and all mixed structures were optimized by GULP in constant pressure energy minimization calculations, where both the ionic positions and cell parameters are allowed to vary during the geometry optimizations.

The different Ca^{2+} and Mn^{2+} arrangements in the solid solutions lead to large numbers of configurations for any particular composition and simulation cell. We have therefore used the SOD (Site Occupancy Disorder) program[35] to study a series of substitutions of Ca^{2+} by Mn^{2+} in supercells of the hexagonal calcite structure. This program generates the complete configurational space for each composition of the supercell and then extracts the symmetrically inequivalent configurations by considering the symmetry operators of the parent structure, thus reducing the number of configurations to be calculated with GULP (or other programs). Once the configurational energetic spectrum is obtained, we consider that the extent of occurrence of one particular configuration in the disordered solid can be described by a Boltzmann-like probability which is calculated,

Table 1. Potential Parameters Used in This Work[a]

Buckingham potential			
ion pair	A (eV)	ρ (Å)	C (eV Å^6)
Ca−O	1550.0	0.29700	0.0
Mn−O	6348.6	0.22927	0.0
O−O	16372.0	0.21300	3.47

[a] Short-range cutoff is 20 Å. Morse potential: C−O, D = 4.71 eV, a = 3.8 Å^{-1}, r_0 = 1.18 Å. Three body potential: O−C−O, k = 1.69 eV rad^{-2}, Θ_0 = 120°. Four body potential: O−C−O-O, k = 0.1129 eV rad^{-2}, Θ_0 = 180°.

Table 2. Experimental[45−47] and Calculated Structural Properties of $CaCO_3$ and $MnCO_3$[a]

	$CaCO_3$		$MnCO_3$	
property	calculated	experiment	calculated	experiment
V (Å^3)	348.3	367.8	285.6	307.8
a (Å)	4.80	4.99	4.55	4.78
c (Å)	17.48	17.06	15.91	15.56
c/a	3.64	3.42	3.49	3.26
B (GPa)	80.4	76.1	135	126
ΔH_{eq1} (kJ mol^{-1})			273.8	279.3

[a] Volumes refer to the hexagonal unit cell; B is the bulk modulus.

assuming zero external pressure and ignoring vibrational contributions, from the lattice energy E_m of the configuration (the minimum energy of the optimized structure at constant pressure by GULP) and its degeneracy Ω_m (the number of times the configuration is repeated in the complete configurational space):[36−39]

$$P_m = \frac{\Omega_m}{Z} \exp(-E_m/k_B T) \quad (2)$$

where $m = 1, ..., M$ (M is the number of inequivalent configurations), k_B is Boltzmann's constant, and Z is the configurational partition function

$$Z = \sum_{m=1}^{M} \Omega_m \exp(-E_m/k_B T) \quad (3)$$

In this study the enthalpy of each configuration is simply its lattice energy, since we have not considered any external pressure in the calculations, and we have ignored vibrational contributions to the enthalpy (see discussion in next section). Then the enthalpy per formula unit H at each composition is calculated as an average in the configurational space

$$H = \frac{1}{N} \sum_{m=1}^{M} P_m H_m = \frac{1}{N} \sum_{m=1}^{M} P_m E_m \quad (4)$$

where N is the number of formula units in the supercell, while the configurational free energy G and the entropy S can be obtained from the partition function Z

$$G = -\frac{1}{N} k_B T \ln Z \quad (5)$$

$$S = \frac{H - G}{T} = -\frac{1}{N} k_B \sum_{m=1}^{M} P_m \ln \frac{P_m}{\Omega_m} \quad (6)$$

It is worth noting that, although the calculated enthalpies of disordered systems tend to converge very rapidly with the size of the simulation cell, the convergence of free energies and entropies is much slower.[40] Therefore, our calculations, which are based on relatively small supercells, can provide precise enthalpies, while the calculated entropies are only used here to assess the degree of disorder in the solutions. The degree of convergence of the entropies with the size of the supercell is discussed below based on the difference between the full-disorder entropy for the given supercell

$$S_{max}(x, N) = \frac{1}{N} k_B \ln \frac{N!}{[Nx]![N(1-x)]!} \quad (7)$$

and the exact full-disorder result

$$S_{ideal}(x) = \lim_{N \to \infty} S_{max}(x, N) = -k_B[x \ln x + (1-x) \ln(1-x)] \quad (8)$$

Any property A_m defined for each configuration m can be averaged over the configurational ensemble as

$$A = \sum_{m=1}^{M} P_m A_m \quad (9)$$

but the interpretation of this average should be done carefully. When the averaging of system properties is performed in the reduced space of inequivalent configurations, each configuration m represents a set of Ω_m equivalent configurations, and therefore the property A_m must be the same for all configurations in that set. For example, if $\mathbf{a}_m$ and $\mathbf{b}_m$ are the equilibrium cell vectors for each inequivalent configuration m, the average value of the cell parameter a corresponding to the disordered crystal cannot be calculated as the direct average of the $|\mathbf{a}_m|$ values, as this result could be different from the direct average of the $|\mathbf{b}_m|$ values, breaking the rotational symmetry of the hexagonal cell. Therefore we have calculated the a cell parameter by using the equation:[41]

$$a = \left(\sum_{m=1}^{M} P_m |\mathbf{a}_m \times \mathbf{b}_m| \right)^{1/2} \quad (10)$$

since the absolute value of the vector product $\mathbf{a}_m \times \mathbf{b}_m$ is invariant within a set of equivalent configurations. The c cell parameter was obtained directly by configurational averaging of the $|\mathbf{c}_m|$ values.

Table 3. Total Number of Configurations (W) and Number of Symmetrically Inequivalent Configurations (M) for Each Composition $Mn_xCa_{1-x}CO_3$ in 2 × 2×1 and 3 × 3×1 Supercells[a]

cell composition	x or $1-x$	W	M
$A_{24}(CO_3)_{24}$	0	1	1
$A_{23}B(CO_3)_{24}$	0.042	24	1
$A_{22}B_2(CO_3)_{24}$	0.083	276	7
$A_{21}B_3(CO_3)_{24}$	0.125	2024	20
$A_{20}B_4(CO_3)_{24}$	0.167	10626	102
$A_{19}B_5(CO_3)_{24}$	0.208	42504	317
$A_{18}B_6(CO_3)_{24}$	0.250	134596	1033
$A_{17}B_7(CO_3)_{24}$	0.292	346104	2467
$A_{16}B_8(CO_3)_{24}$	0.333	735471	5330
$A_{53}B(CO_3)_{54}$	0.019	54	1
$A_{52}B_2(CO_3)_{54}$	0.037	1431	11
$A_{51}B_3(CO_3)_{54}$	0.056	24804	86
$A_{50}B_4(CO_3)_{54}$	0.074	316251	1051

[a] A and B stand for either Ca or Mn.

We have considered here cation substitutions in the 2 × 2 × 1 and 3 × 3 × 1 supercells of the hexagonal unit cell of calcite, including 24 and 54 cation sites respectively. The extension along the x/y axes is studied as $a < c$ in the unit cell and the interactions of cations in neighboring cells thus could have more effect in this direction. The total number of configurations and symmetrically inequivalent configurations for these supercells are listed in Table 3, where x is the molar fraction of Mn in the $Mn_xCa_{1-x}CO_3$ solid solutions. For the 2 × 2 × 1 supercell, the full spectrum of configurations was not calculated for compositions $0.33 < x < 0.67$ due to the still prohibitive computational cost. Instead, we employed a random sampling method to study the configurations with $x = 0.5$, and checked the convergence of the calculated properties with respect to the sample size. The 3 × 3 × 1 supercell was only employed at low concentrations to test convergence with respect to cell size.

RESULTS AND DISCUSSION

It is immediately clear from our calculations that all configurational spectra are very wide, i.e., there are significant differences in energies among configurations with the same composition, thus suggesting that full disorder is unlikely at equilibrium conditions. For example, for the Mn concentration $x = 1/6$, the energies in the full configurational ensemble and the associated

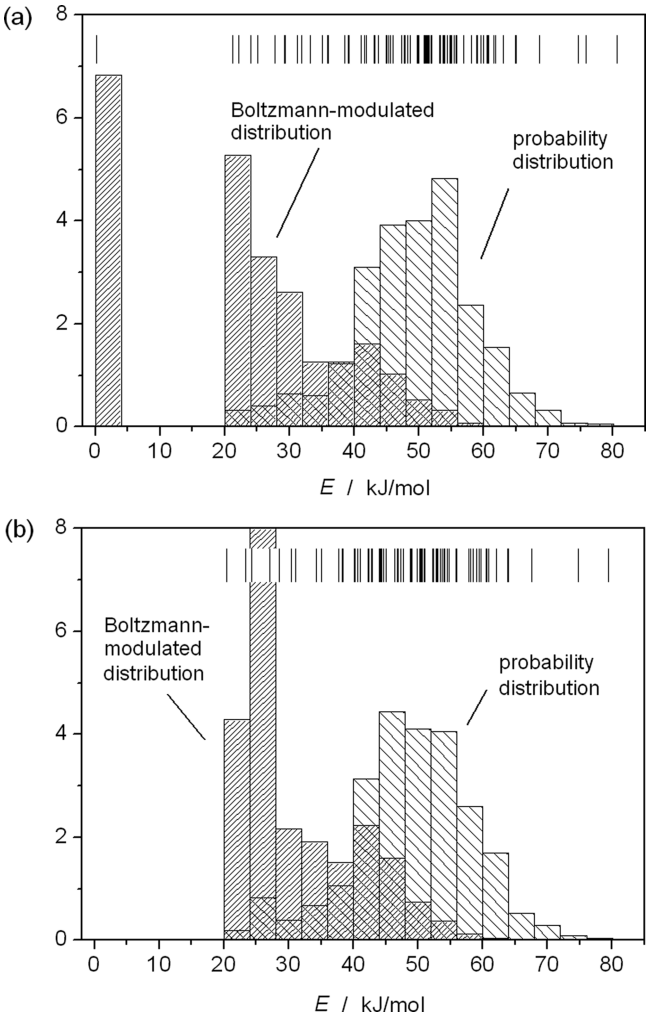

Figure 1. Probability distribution and Boltzmann-modulated (at 700 K) probability distribution of the energies calculated for configurations with composition $x = 1/6$ in the $2 \times 2 \times 1$ supercell using (a) the full configurational ensemble for this supercell and (b) a set of 500 random configurations. The short vertical lines are the energy values in the configurational spectrum.

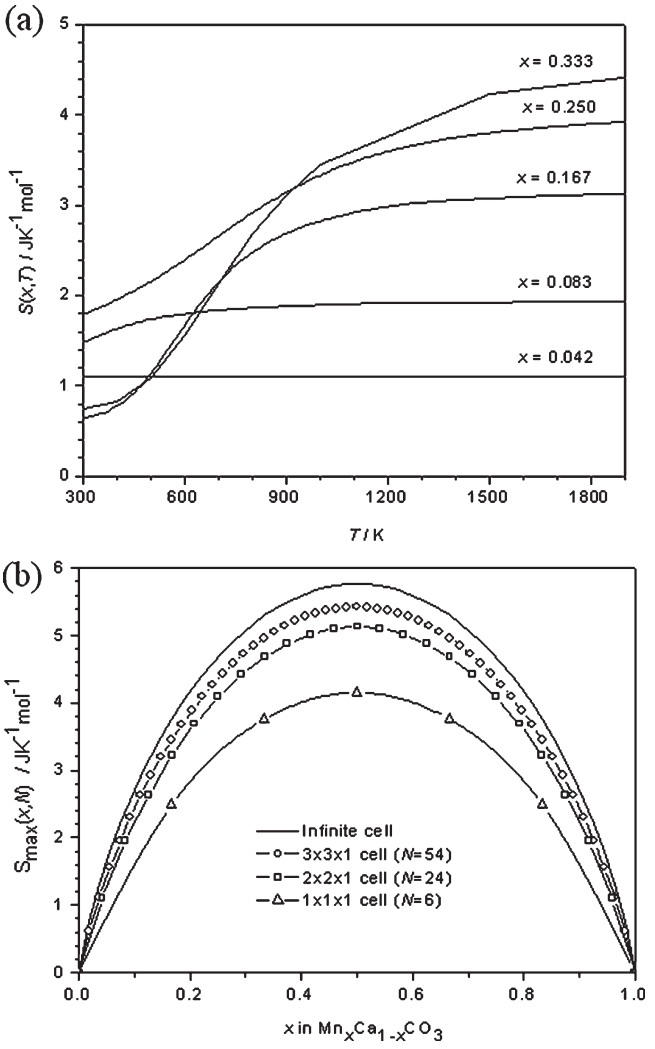

Figure 2. (a) Variation of the configurational entropy with temperature calculated in a $2 \times 2 \times 1$ supercell. (b) Variation of the maximum configurational entropy (in the full disorder limit) with the supercell size.

probability distribution (taking degeneracies into account) are shown in Figure 1a. The difference between the lowest-energy and the highest-energy configuration is ~80 kJ/mol. These energy differences will lead to significant deviation from a random distribution of cations upon equilibration at any reasonable temperature. Figure 1a also shows the probability distribution modulated by a Boltzmann function (we used $T = 700$ K here), to reflect better the relative contribution of configurations to ensemble averages at equilibrium. The lowest-energy configuration has a very high weight, while the contribution from higher-energy configurations decreases rapidly with their energy. This analysis also highlights the risk of random configurational sampling methods in the study of systems with partial ordering: if the lowest-energy configuration is missed (which is not difficult, because they tend to be highly symmetric configurations with very low degeneracy), the probability distribution is significantly affected. For example, in Figure 1b we have plotted the energies and probability distributions for a random selection of 500 configurations for the composition $x = 1/6$. This number is higher than the number of symmetrically inequivalent configurations (102) for this composition and supercell, but still is not enough to describe the energy distribution properly, because the random sampling missed the configurational groundstate.

A quantitative measure of the degree of cation ordering in the system is provided by the configurational entropy, as given by eq 6. Figure 2a shows its variation with temperature for $Mn_xCa_{1-x}CO_3$ with $x < 0.33$, as calculated in a $2 \times 2 \times 1$ supercell. The composition $x = 0.042$ corresponds to only one Mn^{2+} substitution of any of the 24 equivalent Ca^{2+} in the supercell, therefore all 24 configurations are equivalent in this case and the configurational entropy is constant (at its maximum value for this supercell) with temperature. For the other Mn compositions, where there are a number of possible inequivalent distributions of the cations, the configurational entropy gradually approaches the maximum value when temperature is increased. The variation of the configurational entropy of the $(Mn,Ca)CO_3$ system with temperature indicates that a significant level of ordering should be present at low temperatures (say, below 1000 K), if there is full configurational equilibrium. It is important to note that for the supercell size used here ($N = 24$) the

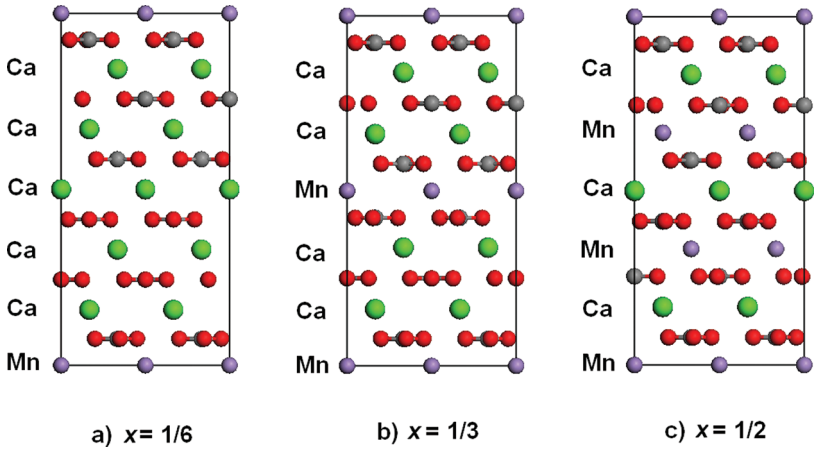

Figure 3. Structures of the most stable configurations for $x = n/6$ ($n = 1,2,3$). The lowest-energy structures for $n = 4$ and 5 can be obtained from the ones with $n = 2$ and 1, respectively, if Ca and Mn positions are swapped. The $n = 3$ case ($x = 1/2$) corresponds to the ordered mineral kutnahorite.

absolute entropy values are not totally converged. To illustrate this point, we show in figure 2b the variation of the maximum entropy for different cell sizes in comparison with the exact result in the full disorder limit, for which an analytical expression exists (eq 8). For the $2 \times 2 \times 1$ supercell ($N = 24$) the high temperature limit is in significant error (e.g., by 12% for $x = 0.25$). However, although not fully converged, the calculated configurational entropies are very useful to assess the level of disorder to be expected in the system at equilibrium conditions.

In order to understand the driving force toward ordering, we have identified the most stable (lowest energy) configuration for each composition. Figure 3, panels a and b, shows the lowest-energy configurations for $x = 1/6$ and $1/3$, respectively. A clear pattern emerges here: Mn dopants prefer to concentrate in the same layer perpendicular to the hexagonal cell main (c) axis, and at the same time, these full-Mn layers prefer to be as far as possible from each other. These ordered patterns are consistent with a simple interaction model where Mn−Mn interactions are favorable within (0001) layers but unfavorable between layers, as suggested recently by Katsikopoulos et al. based on empirical evidence.[15] This tendency is quite strong and remains valid for all compositions in the solid solutions, as we will discuss below.

Further insight into the thermodynamics of mixing in this system can be obtained by calculating the enthalpies of mixing as a function of the Mn^{2+} molar fraction x

$$\Delta H_{\mathrm{mix}} = E[Mn_xCa_{1-x}CO_3] - (1-x)E[CaCO_3] - xE[MnCO_3] \quad (11)$$

where $E[Mn_xCa_{1-x}CO_3]$ is the average lattice energy of the $(Mn,Ca)CO_3$ mixed system, and $E[CaCO_3]$ and $E[MnCO_3]$ are the lattice energies of the pure calcite and rhodochrosite, respectively. We have checked that the errors associated with the use of the internal energies E (instead of the proper enthalpies H, which include zero-point and heat capacity contributions) are negligible. For example, for $Mn_{1/24}Ca_{23/24}CO_3$ at 298 K, the enthalpy of mixing changes from 0.707 to 0.699 kJ mol^{-1} when vibrational contributions are considered, which is a change of only ~1%. This is not surprising, as vibrational contributions to mixing enthalpies (although not necessarily to mixing free energies) tend to be very small.[41,42]

We first discuss the energetics of mixing in the fully disordered $Mn_xCa_{1-x}CO_3$ system for compositions $x < 1/3$. All the equilibrium

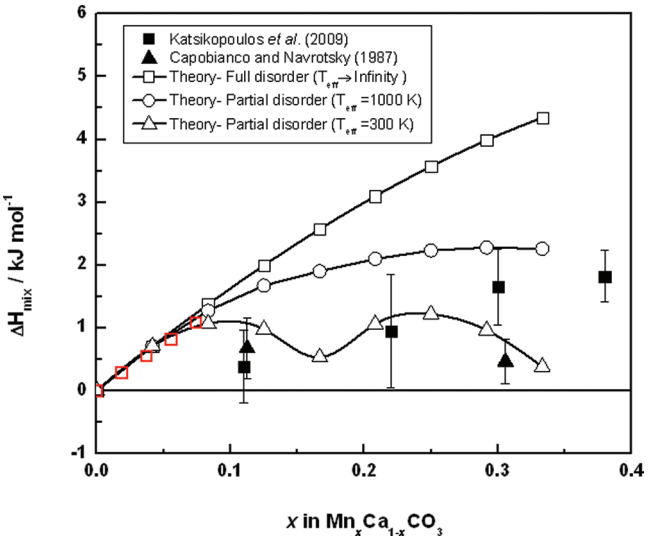

Figure 4. Calculated and experimental mixing enthalpies for the Ca-rich $Mn_xCa_{1-x}CO_3$ solid solution. The empty squares in red color correspond to calculations in the full disorder limit with the $3 \times 3 \times 1$ supercell.

geometries and energies of the Ca-rich configurations were calculated, and the average energy was taken in the high temperature limit ($T \rightarrow \infty$), i.e., configurations were only weighted by their degeneracies, regardless of their energies. Figure 4 shows the enthalpies of mixing ΔH_{mix} as a function of Mn content, together with experimental findings by other authors. The calculated ΔH_{mix} values for the fully disordered system (empty squares) are clearly positive, which is also seen in experiments. However, our theoretical values seem to be too high when compared with the calorimetric measurements by Katsikopoulos et al.[15] and Capobianco and Navrotsky.[14] This discrepancy can arise from systematic errors in either the simulations or the experiments. The consideration of a larger simulation cell ($3 \times 3 \times 1$, red empty squares in Figure 4), does not seem to alter significantly the mixing enthalpy values. However, it is also possible to explain this discrepancy by considering that there may be some degree of ordering in the experimental samples, which reduces their mixing enthalpies with respect to the full disorder

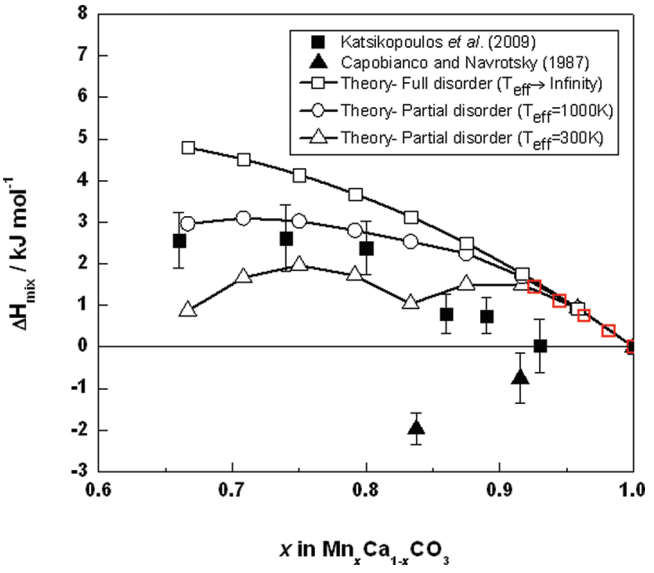

Figure 5. Calculated and experimental mixing enthalpies for the Mn-rich $Mn_xCa_{1-x}CO_3$ solid solution. The empty squares in red correspond to calculations in the full disorder limit with the 3 × 3 × 1 supercell.

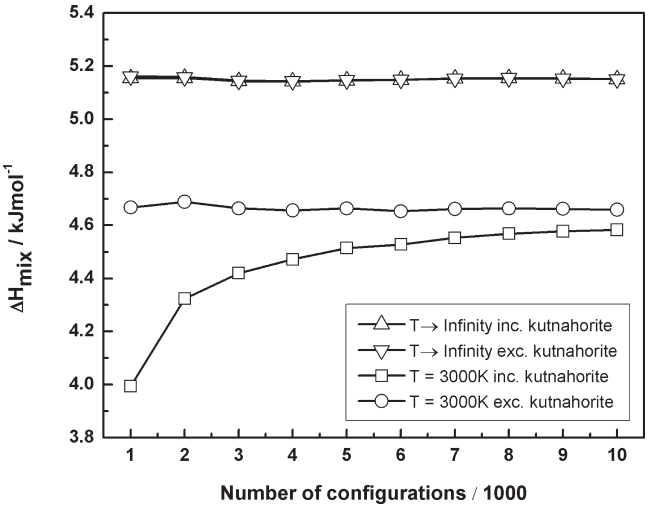

Figure 6. Variation of enthalpy of mixing with different number of $Mn_{0.5}Ca_{0.5}CO_3$ configurations at 3000 K and infinitely high temperature.

limit. We note here that although Katsikopoulos et al.[15] were able to rule out kutnahorite-type ordering in their samples, based on the absence of superstructure reflections in the X-ray diffraction patterns, diffraction techniques are not well suited to assess the level of disorder in poorly ordered samples, say, in comparison with the ideal disorder limit. Therefore, our suggestion of imperfect disorder in the samples does not conflict with the available experimental information. In Figure 4 we also plot the enthalpies of mixing for the $Mn_xCa_{1-x}CO_3$ system considering full equilibration at 300 and 1000 K. The theoretical values of ΔH_{mix} of the partially ordered systems are lower as a result of higher weighting of the lower-energy configurations. In this case, the theoretical prediction agrees much better with the experimental results, especially when considering the wide error bars of the experimental data points.

We now discuss Ca-substituted rhodochrosite, i.e. $Mn_xCa_{1-x}CO_3$ solid solutions with high concentrations of Mn^{2+} ($x > 2/3$). In this case, the most stable configurations at each composition are again those which maximize the intralayer homogeneity and interlayer heterogeneity of cations (the most stable configurations for $x = 2/3$ and $x = 5/6$ are equivalent to those depicted in Figures 2 (a) and (b), respectively, but with Ca and Mn positions swapped). The enthalpies of mixing for $x > 2/3$ are shown in Figure 5 in comparison with experiments. As for the Ca-rich compositions, the consideration of a larger supercell (3 × 3 × 1) does not change significantly the values of the mixing enthalpies. The ΔH_{mix} for the incorporation of Ca^{2+} in rhodochrosite is somewhat higher than for Mn^{2+} impurities in calcite; that is, it is energetically more expensive to substitute Ca^{2+} into rhodochrosite than Mn^{2+} into calcite, due to the larger ionic radius of Ca^{2+} compared to Mn^{2+}. It is generally found that smaller cations can substitute more easily in positions normally occupied by larger cations, which causes less elastic strain in the lattice than the opposite scenario.[33,34,43] Similar to the incorporation of Mn^{2+} in calcite, the positive values of the calculated ΔH_{mix} in the fully disordered $(Mn,Ca)CO_3$ systems are somewhat higher than the experimental measurements. Again, when we consider partial cation ordering in the systems, the enthalpy of mixing decreases and becomes closer to the experimental measurements by Katsikopoulos et al.[15] It is interesting to note that earlier experiments by Capobianco and Navrotsky[14] had reported negative values of ΔH_{mix} for these Mn-rich compositions. Our calculated mixing enthalpies, as well as those obtained in the simulations by Vinograd et al., are positive for these compositions, in agreement with the most recent experiments. As pointed out by Katsikopoulos et al.,[15] it seems likely that these measurements were performed on samples with significant levels of ordering.

We have also investigated the structure, cation ordering behavior and stability in $Mn_{0.5}Ca_{0.5}CO_3$ at different temperatures. The fully ordered $Mn_{0.5}Ca_{0.5}CO_3$ structure has been detected in the natural mineral kutnahorite,[44] which exhibits dolomite-like cation ordering, where Mn and Ca layers alternate with layers of carbonate ions along the crystallographic *c*-axis (see Figure 3c). The composition $x = 0.5$ leads to a total of almost three million configurations in the 2 × 2 × 1 supercell, and this is computationally too expensive to calculate directly. We have therefore employed a random sampling method to generate a series of groups, where the number of configurations increases in successive groups from 1000 to 10000. We calculated the enthalpy of mixing ΔH_{mix} based on the equilibrium geometries and energies of all of the configurations in each group. We find that the configurational spectrum is very dense, with many configurations having very similar energies. However, in all cases, the lowest energy arrangement of cations corresponds to the dolomite-like kutnahorite structure of Figure 3c. The least stable configuration found in our random sampling had a lattice energy 56 kJ mol^{-1} (2.3 kJ mol^{-1} per formula unit) higher than the ordered kutnahorite structure.

In order to test the convergence of our results with respect to the configuration sample size, we have checked that the calculated mixing enthalpy at high temperature does not depend on the inclusion of the kutnahorite configuration in the sample (Figure 6). In the limit of full disorder ($T \rightarrow \infty$), the exclusion of the kutnahorite configuration does not make any difference on the average enthalpy even for relatively small sample sizes (e.g., 1000 configurations). However, if equilibration at a finite

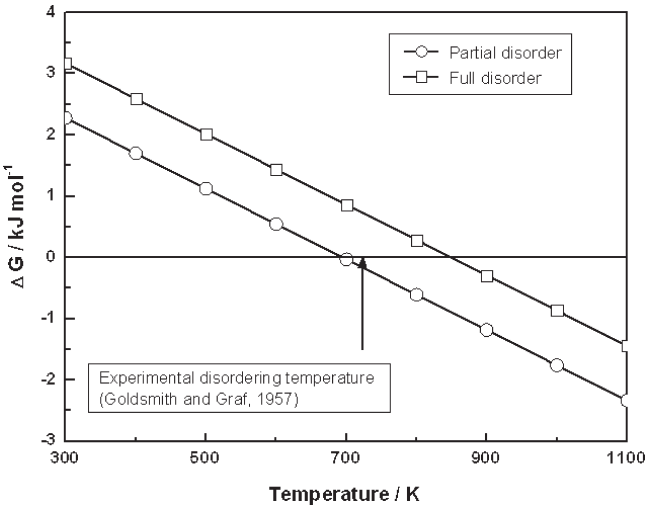

Figure 7. Difference in free energy ΔG between the disordered $Mn_{0.5}Ca_{0.5}CO_3$ phase and ordered kutnahorite as a function of temperature. The enthalpy for the partially disordered structure was obtained using Boltzmann averaging at an effective temperature of T = 3000 K.

temperature (e.g., 3000 K) is allowed, many more configurations are required to produce a robust result. For ~10 000 configurations, the average is practically independent of the presence of the kutnahorite configuration. Therefore, a sample of this size can be assumed to provide a good representation of the energy distribution in the full configurational spectrum at this temperature.

Figure 6 also shows that there is a significant difference in the average enthalpy between the fully disordered solid solution, where all of the configurations enter with the same weight, and one with some level of ordering, where the lowest-energy configurations have increased weights. The temperature of 3000 K in this case does not represent a real thermal effect, but it is introduced to show the increasing presence of lower-energy cation arrangements, which is possible even in a sample that is not in configurational equilibrium. As in the cases of Ca-rich and Mn-rich solid solutions, we will show now that the assumption of such a moderate degree of cation ordering leads to better agreement of our calculations with experimental results. We have evaluated the transition temperature of kutnahorite to disordered $Mn_{0.5}Ca_{0.5}CO_3$, by computing the free energy difference between the disordered and ordered phases

$$\Delta G = H_{\text{disordered}} - TS_{\text{disordered}} - H_{\text{ordered}} \quad (12)$$

where $H_{\text{disordered}}$ and $S_{\text{disordered}} = k_B \ln 2 = 5.763$ J/mol K are the enthalpy and the ideal entropy of the disordered 50:50 solid solution and H_{ordered} is the enthalpy of the ordered kutnahorite phase. The enthalpy of the disordered $Mn_{0.5}Ca_{0.5}CO_3$ solid solution was evaluated in eq 4 both in the limit of full disorder and in the case of some incipient ordering, corresponding to the 3000 K calculation explained above. Figure 7 shows that the disordered phase is predicted to become stable at 849 K if the full disorder enthalpy is used. However, allowing for some degree of ordering in the solid solution reduces the transition temperature to 695 K, which is in better agreement with the experimental disordering temperature of kutnahorite (723 K) given by Goldsmith and Graf.[9] Thus, again, agreement between theory and experiment is better if we assume that the solid solutions, which are considered to be disordered experimentally, are not really fully disordered but contain some small bias toward lower energy configurations.

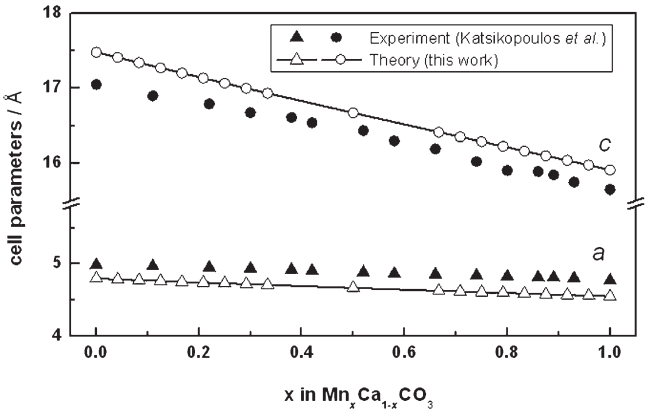

Figure 8. Variation of the lattice parameters of $Mn_xCa_{1-x}CO_3$ as a function of composition, in comparison with experiment (Katsikopoulos et al.[15]).

Finally, we have calculated the average lattice parameters of the fully disordered calcite-rhodochrosite systems through eqs 9 and 10. The variation of the lattice parameters a (where $a = b$) and c with Mn^{2+} composition is plotted in Figure 8, which shows that both lattice parameters decrease with increasing Mn^{2+} substitution, as expected from the smaller ionic radius of Mn^{2+} compared to Ca^{2+}, and in agreement with experiment.[9,10,13,15] The small deviation from the linear Vegard's law reported in the paper by Katsikopoulos et al.[15] for intermediate compositions was not obtained in our simulations in the full disorder limit, suggesting that the nonlinear behavior is most likely associated with a deviation from perfect disorder in the experimental samples, consistent with our discussion above regarding partial ordering.

CONCLUSIONS

We have employed atomistic simulation techniques to study the thermodynamic mixing properties of $CaCO_3$—$MnCO_3$ solid solutions in the whole range of compositions. According to our calculations, the fully disordered solid solution has positive enthalpies of mixing throughout the range of compositions, which, however, decrease when partial configurational ordering is considered. Configurations with some small degree of ordering generally lead to better agreement with experiment. Our results indicate that experimental measurements, where negative mixing enthalpies for the $CaCO_3$—$MnCO_3$ solid solution were obtained for Mn-rich compositions, are most probably due to cation ordering in the experimental samples.

For the intermediate composition of Mn/Ca = 1, the ordered structure of kutnahorite is the most stable configuration. Kutnahorite becomes less stable than a fully disordered structure at 849 K, but the predicted disordering temperature decreases to 695 K, in better agreement with experiment (723 K) if a transition to a structure with some level of ordering is considered. Our results suggest that, although most synthetic and mineral samples are very disordered due to kinetic inhibition of the interlayer ordering pattern, this inhibition is never complete: lower energy cation arrangements are likely to occur with higher probabilities than those expected from a fully disordered distribution. The geologically important $CaCO_3$—$MnCO_3$ solutions are thus not

equilibrated at ambient temperature, neither are they fully random; they are probably better described by pseudo-equilibrium conditions at high (but not infinite) temperatures, which should be taken into account when evaluating the thermodynamics of Mn incorporation in calcite under environmental conditions.

■ ACKNOWLEDGMENT

Q.W. is grateful to the China Scholarship Council for financial support and University College London for an Overseas Research Studentship. We also thank the EU-funded "Mineral Nucleation and Growth Kinetics (MIN-GRO) Marie-Curie Research and Training Network" (Grant No. MRTN-CT-2006-035488) for funding.

■ REFERENCES

(1) Davidsson, L.; Cederblad, A.; Lonnerdal, B.; Sandstrom, B. *Am. J. Dis. Child.* **1989**, *143*, 823.
(2) Khoe, G. H.; Waite, T. D. *Environ. Technol. Lett.* **1989**, *10*, 479.
(3) Davidsson, L.; Cederblad, A.; Lonnerdal, B.; Sandstrom, B. *Am. J. Clin. Nutr.* **1989**, *49*, 170.
(4) El-Korashy, S. A. *J. Mater. Sci.* **2003**, *38*, 1709.
(5) Graven, E. H.; Attoe, O. J.; Smith, D. *Proc. Soil Sci. Soc. Am.* **1965**, *29*, 702.
(6) Stipp, S. L. S.; Konnerup-Madsen, J.; Franzreb, K.; Kulik, A.; Mathieu, H. J. *Nature* **1998**, *396*, 356.
(7) Zachara, J. M.; Cowan, C. E.; Resch, C. T. *Geochim. Cosmochim. Acta* **1991**, *55*, 1549.
(8) Goldsmith, J. R. *Rev. Mineral. Geochem.* **1983**, *11*, 49.
(9) Goldsmith, J. R.; Graf, D. L. *Geochim. Cosmochim. Acta* **1957**, *11*, 310.
(10) DeCapitani, C.; Peters, T. *Contrib. Mineral. Petrol.* **1981**, *76*, 394.
(11) Winter, G. A.; Essene, E. J.; Peacor, D. R. *Am. Mineral.* **1981**, *66*, 278.
(12) Pedersen, T. F.; Price, N. B. *Geochim. Cosmochim. Acta* **1982**, *46*, 59.
(13) McBeath, M. K.; Rock, P. A.; Casey, W. H.; Mandell, G. K. *Geochim. Cosmochim. Acta* **1998**, *62*, 2799.
(14) Capobianco, C.; Navrotsky, A. *Am. Mineral.* **1987**, *72*, 312.
(15) Katsikopoulos, D.; Fernandez-Gonzalez, A.; Prieto, M. *Geochim. Cosmochim. Acta* **2009**, *73*, 6147.
(16) Parker, S. C.; Kelsey, E. T.; Oliver, P. M.; Titiloye, J. O. *Faraday Discuss.* **1993**, 75.
(17) de Leeuw, N. H.; Parker, S. C. *J. Chem. Soc. Faraday T* **1997**, *93*, 467.
(18) de Leeuw, N. H.; Parker, S. C. *J. Phys. Chem. B* **1998**, *102*, 2914.
(19) Fisler, D. K.; Gale, J. D.; Cygan, R. T. *Am. Mineral.* **2000**, *85*, 217.
(20) Cygan, R. T.; Wright, K.; Fisler, D. K.; Gale, J. D.; Slater, B. *Mol. Simul.* **2002**, *28*, 475.
(21) Austen, K. F.; Wright, K.; Slater, B.; Gale, J. D. *Phys. Chem. Chem. Phys.* **2005**, *7*, 4150.
(22) Vinograd, V. L.; Burton, B. P.; Gale, J. D.; Allan, N. L.; Winkler, B. *Geochim. Cosmochim. Acta* **2007**, *71*, 974.
(23) Vinograd, V. L.; Sluiter, M. H. F.; Winkler, B. *Phys. Rev. B* **2009**, *79*, 9.
(24) Vinograd, V. L.; Paulsen, N.; Winkler, B.; van de Walle, A. *Calphad* **2010**, *34*, 113.
(25) Born, M.; Huang, K. *Dynamical theory of crystal lattices*; Oxford University Press: Oxford, U.K., 1954.
(26) Dick, B. G.; Overhauser, A. W. *Phys. Rev.* **1958**, *112*, 90.
(27) Pavese, A.; Catti, M.; Price, G. D.; Jackson, R. A. *Phys. Chem. Miner.* **1992**, *19*, 80.
(28) Pavese, A.; Catti, M.; Parker, S. C.; Wall, A. *Phys. Chem. Miner.* **1996**, *23*, 89.
(29) Catti, M.; Pavese, A.; Price, G. D. *Phys. Chem. Miner.* **1993**, *19*, 472.
(30) Gale, J. D. *J. Chem. Soc., Faraday Trans.* **1997**, *93*, 629.
(31) Gale, J. D. *Z. Kristallogr.* **2005**, *220*, 552.
(32) Gale, J. D.; Rohl, A. L. *Mol. Simul.* **2003**, *29*, 291.
(33) de Leeuw, N. H. *J. Phys. Chem. B* **2002**, *106*, 5241.
(34) de Leeuw, N. H.; Parker, S. C. *J. Chem. Phys.* **2000**, *112*, 4326.
(35) Grau-Crespo, R.; Hamad, S.; Catlow, C. R. A.; de Leeuw, N. H. *J. Phys. - Condens. Mat.* **2007**, *19*, 256201.
(36) Grau-Crespo, R.; de Leeuw, N. H.; Catlow, C. R. A. *Chem. Mater.* **2004**, *16*, 1954.
(37) Grau-Crespo, R.; De Leeuw, N. H.; Hamad, S.; Waghmare, U. V. *Proc. R. Soc. A-Math. Phys. Eng. Sci.* **2011**, *467*, 1925.
(38) Smith, K. C.; Fisher, T. S.; Waghmare, U. V.; Grau-Crespo, R. *Phys. Rev. B* **2010**, *82*, 134109.
(39) Grau-Crespo, R.; Al-Baitai, A. Y.; Saadoune, I.; De Leeuw, N. H. *J. Phys.- Condens. Matter* **2010**, *22*, 255401.
(40) Todorov, I. T.; Allan, N. L.; Lavrentiev, M. Y.; Freeman, C. L.; Mohn, C. E.; Purton, J. A. *J. Phys. - Condens. Matter* **2004**, *16*, S2751.
(41) Benny, S.; Grau-Crespo, R.; De Leeuw, N. H. *Phys. Chem. Chem. Phys.* **2009**, *11*, 808.
(42) Ruiz-Hernandez, S. E.; Grau-Crespo, R.; Ruiz-Salvador, A. R.; De Leeuw, N. H. *Geochim. Cosmochim. Acta* **2010**, *74*, 1320.
(43) McLean, D. *Grain boundaries in metals*; Clarendon Press: Oxford, U.K., 1957.
(44) Frondel, C.; Bauer, L. H. *Am. Mineral.* **1955**, *40*, 748.
(45) Lide, D. R. *Handbook of Chemistry and Physics*, 81 ed.; CRC: London, 2000.
(46) Deer, W. A.; Howie, R. A.; Zussman, J. *Introduction to the Rock Forming Minerals*; Longman Harlow: London, 1992.
(47) Ono, S. *Mineral. Mag.* **2007**, *71*, 105.